Supporting information

Unusual deprotonated alkynyl hydrogen bonding in metal-supported hydrocarbon assembly

*Yi-Qi Zhang,[1†] Jonas Björk,[2†] Peter Weber,[1] Raphael Hellwig,[1] Katharina Diller,[1] Anthoula C. Papageorgiou,[1] Seung Cheol Oh,[1] Sybille Fischer,[1] Francesco Allegretti,[1] Svetlana Klyatskaya,[3] Mario Ruben,[3,4] Johannes V. Barth,[1] and Florian Klappenberger[1,]**

[1] Physik Department E20, Technische Universität München, 85748 Garching, Germany

[2] Department of Physics, Chemistry and Biology (IFM), Linköping University, 58183 Linköping, Sweden

[3] Institute of Nanotechnology (INT), Karlsruhe Institute of Technology (KIT), 76344 Eggenstein-Leopoldshafen, Germany

[4] IPCMS-CNRS, Université de Strasbourg, 23 rue de Loess, 67034 Strasbourg, France

†These authors contributed equally to this work.
*E-mail: florian.klappenberger@tum.de

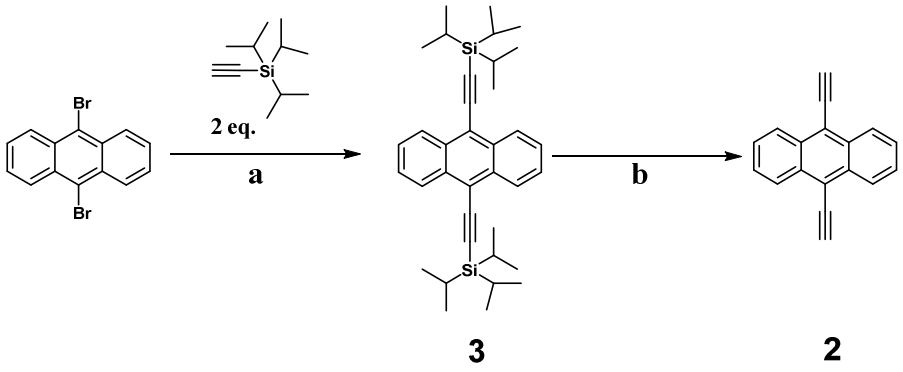

Scheme S1. Synthesis of **2**, conditions: (a) $Pd(PPh_3)_2Cl_2$, CuI, Ph_3P, *i*-Pr_2NH/THF, 90°C, 80%; (b) 1M TBAF, THF/MeOH, 0°C, 85%.

Synthesis

Reactions requiring an inert gas atmosphere were conducted under argon, and the glassware was oven-dried (140 °C). THF was distilled from potassium prior to use. Diisopropylamine was distilled over CaH_2 and stored under argon. Commercially available chemicals were used as received. Thin-layer chromatography was performed on aluminum plates precoated with Merck 5735 silica gel 60 F_{254}. Column chromatography was performed with Merck silica gel 60 (230 - 400 mesh). ^1H NMR and ^{13}C NMR spectra were recorded on a Bruker DRX 500 spectrometer; chemical shifts are given in ppm, referenced to residual proton resonances of the solvents. Elemental analyses of carbon, hydrogen, and nitrogen were carried out in a Vario Micro Cube. IR spectra were measured in KBr pellets on MAGNA FTIR 750, Nicolet.

9,10-Diethynyl-anthracene (**2**).

A solution of Bu_4NF in THF (1 M; 0.5 mL, 0.5 mmol) was added to a solution of **3** (1.5 g, 2.78 mmol) in THF (120 mL) under an argon atmosphere. The mixture was stirred for 3.5 h by cooling with ice-bath. The organic solvent was gently distilled off under argon atmosphere. The solid formed was washed by cold methanol and dried in argon atmosphere to afford **1** as a yellow powder (528 mg, 85%).

^{1}H NMR (CD_2Cl_2): 4.21 (s, 2H, -C≡CH), 7.68-7.70 (m, 4H$_{arom}$), 8.64-8.66 (m, 4H$_{arom}$).

^{13}C NMR (CD_2Cl_2): 89.21, 90.52, 118.14, 127.28, 127.57, 132.80

IR (KBr, ν/cm^{-1}): 3295 ($\nu_{C\equiv C\text{-}H}$, s), 3068, 2876 ($\nu_{C\text{-}H}$, vw), 2159 ($\nu_{C\equiv C}$, vw).

Anal. calcd. for $C_{18}H_{10}$: C, 95.55; H, 4.45. Found: C, 95.41; H, 4.58.

9,10-Bis-[(triisopropylsilanyl)-ethynyl]-anthracene (**3**).

9,10-Dibromanthracene (1.68 g, 5.0 mmol), $Pd(PPh_3)_2Cl_2$ (80 mg), CuI (40 mg) and triphenyl posphine (80 mg) were dissolved in THF/diisopropylamine (50/50 mL) under an argon atmosphere. The solution was heated to 95 °C and 2-triisopropylsilylacetylene (TIPSA) (2.30 g, 12.5 mmol) was added and the solution stirred at this temperature for 4 h. After cooling to room temperature, diethyl ether and water were added; the organic phase was separated and washed with water, 10 %-H_2SO_4, water and brine. After drying over $MgSO_4$ and evaporation of the solvent, the crude product was purified by column chromatography on SiO_2 using hexane as eluent (R_f = 0.38) to afford **3** as a yellow powder (2.17 g, 80%).

^{1}H NMR (CD_2Cl_2): 1.30-1.32 (m, 36H, 2 TIPS), 7.65-7.68 (m, 4H$_{arom}$), 8.68-8.70 (m, 4H$_{arom}$).

^{13}C NMR (CD_2Cl_2): 11.91, 19.04, 103.55, 105.57, 119.03, 127.31, 127.55, 132.73.

IR (KBr, ν/cm^{-1}): 2946, 2866 ($\nu_{C\text{-}H}$, vw), 2165 ($\nu_{C\equiv C}$, vw).

Anal. calcd. for $C_{36}H_{50}NSi_2$: C, 80.23; H, 9.35; Si, 10.42. Found: C, 80.21; H, 9.33.

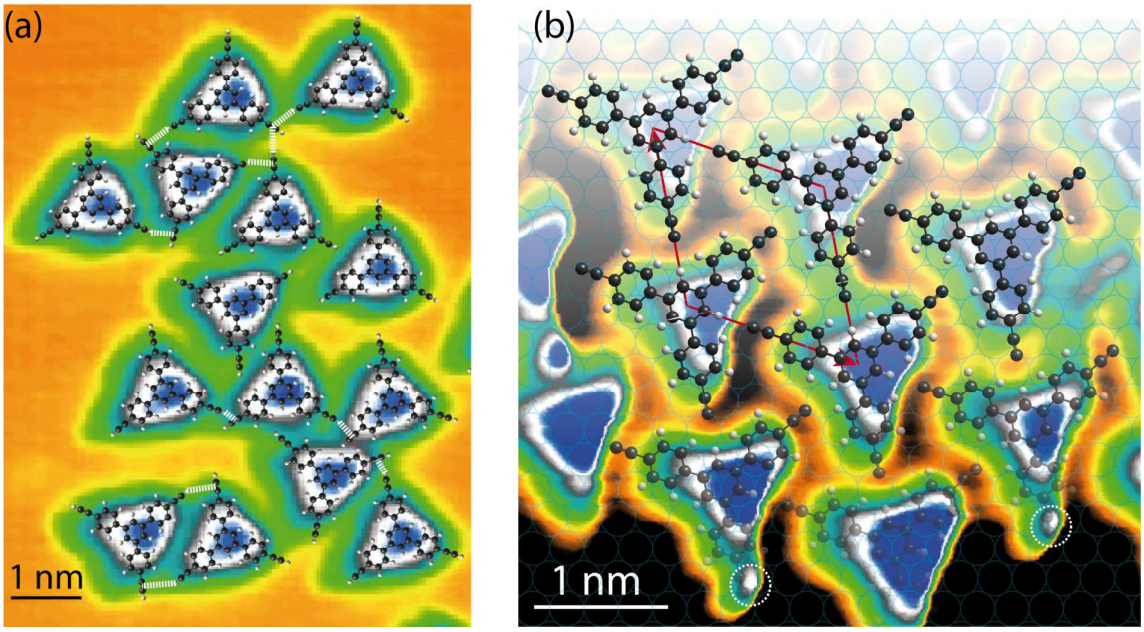

Figure S1. (a) STM image of Ext-TEB on Cu(111) (T_{ann} = 200 K), U_b = -1.0 V, I_t = 0.1 nA, T_{STM} = 5.5 K. The HYPERCHEM gas phase intact Ext-TEB models are superimposed. The dashed lines indicate CH· · ·π interaction. (b) STM image of Ext-TEB network on Cu(111) (T_{ann} = 350 K). The supramolecular unit cell is indicated and the dashed circles indicate possible π-bonded Cu-acetylides. U_b = 1 V, I_t = 0.16 nA, T_{STM} = 5.5 K. The Cu(111) lattice is superimposed as blue circles.

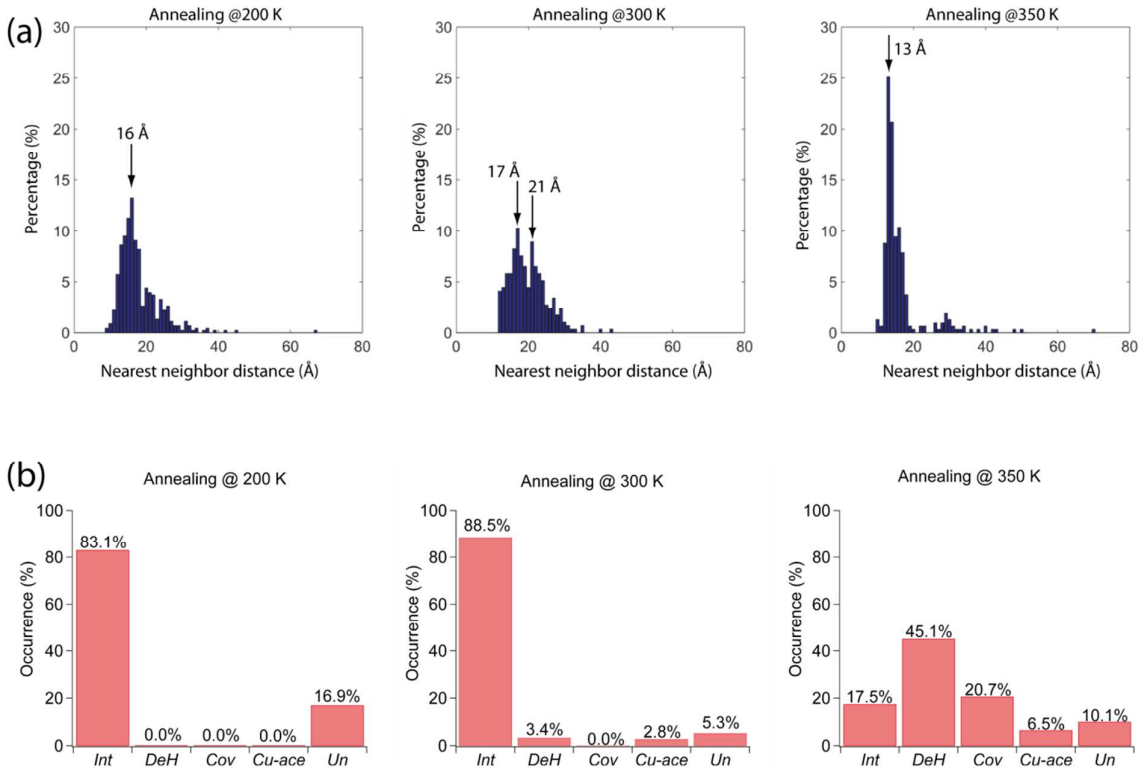

Figure S2. (a) Nearest neighbor distance histograms of the same sample for three different annealing temperatures of 200 K, 300 K and 350 K. (b) Relative occurrence of alkyne moieties of different chemical states at annealing temperature according to (a). A single case indicates the feature of a single alkynyl group. (Abbreviations: *Int* = intact, *DeH* = deprotonated, *Cov* = Covalent, *Cu-ace* = Cu-acetylide, *Un* = unidentified). The unidentified case refers to situations where no depression or protrusion can be seen at the terminal alkynyl due to a short distance to its neighbor. For the sample annealed to 350 K, the terminal alkynes of the molecules within the supramolecular islands are assumed to be deprotonated. The statistics presented in (a) and (b) are extracted from high resolution STM overview images of 512 x 512 pixels corresponding to lateral dimensions of 45 × 45 nm^2. All the images were recorded at 5.5 K.

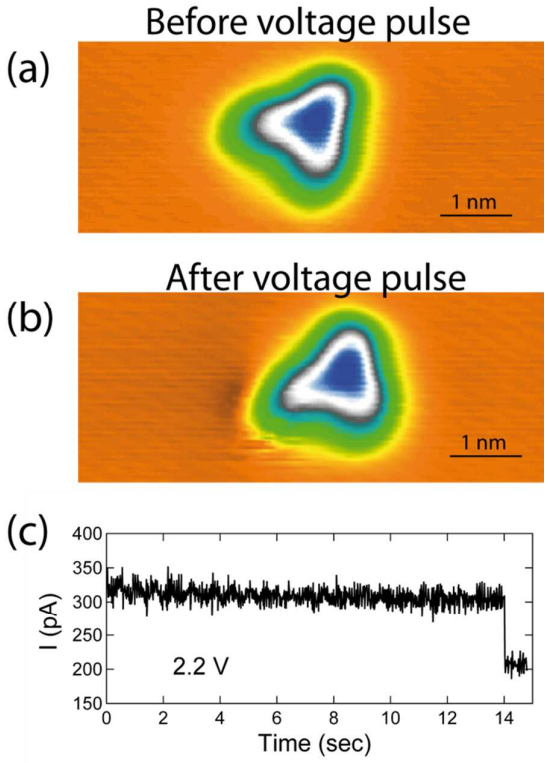

Figure S3. (a, b) STM images (U_b = -1 V, I_t = 0.1 nA) showing tip induced deprotonation of an Ext-TEB molecule on Ag(111) upon a voltage pulse of 2.2 V. (c) Current versus time for the duration of the voltage pulse. The pulse was applied for 15 seconds with open feedback loop.

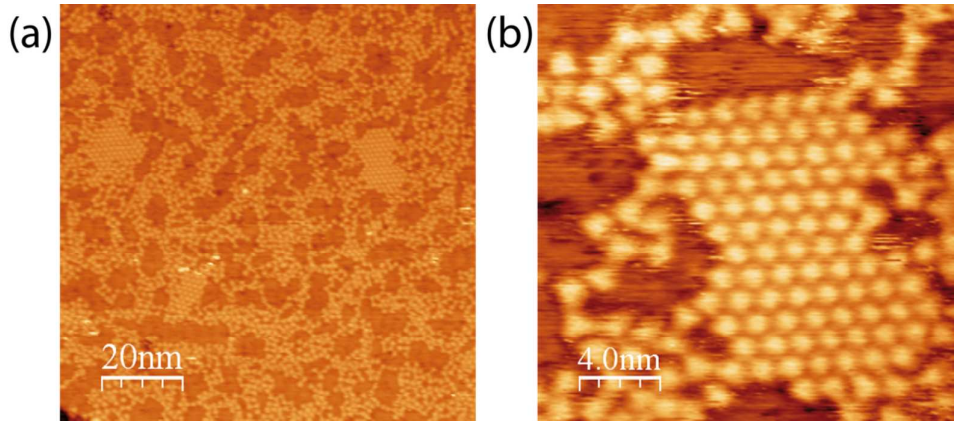

Figure S4. (a) Large-scale STM image of Ext-TEB on Cu(111) recorded at room temperature (300 K). (b) A zoom-in image of a smaller area. Scanning parameters: U_b = 2 V, I_t = 0.3 nA.

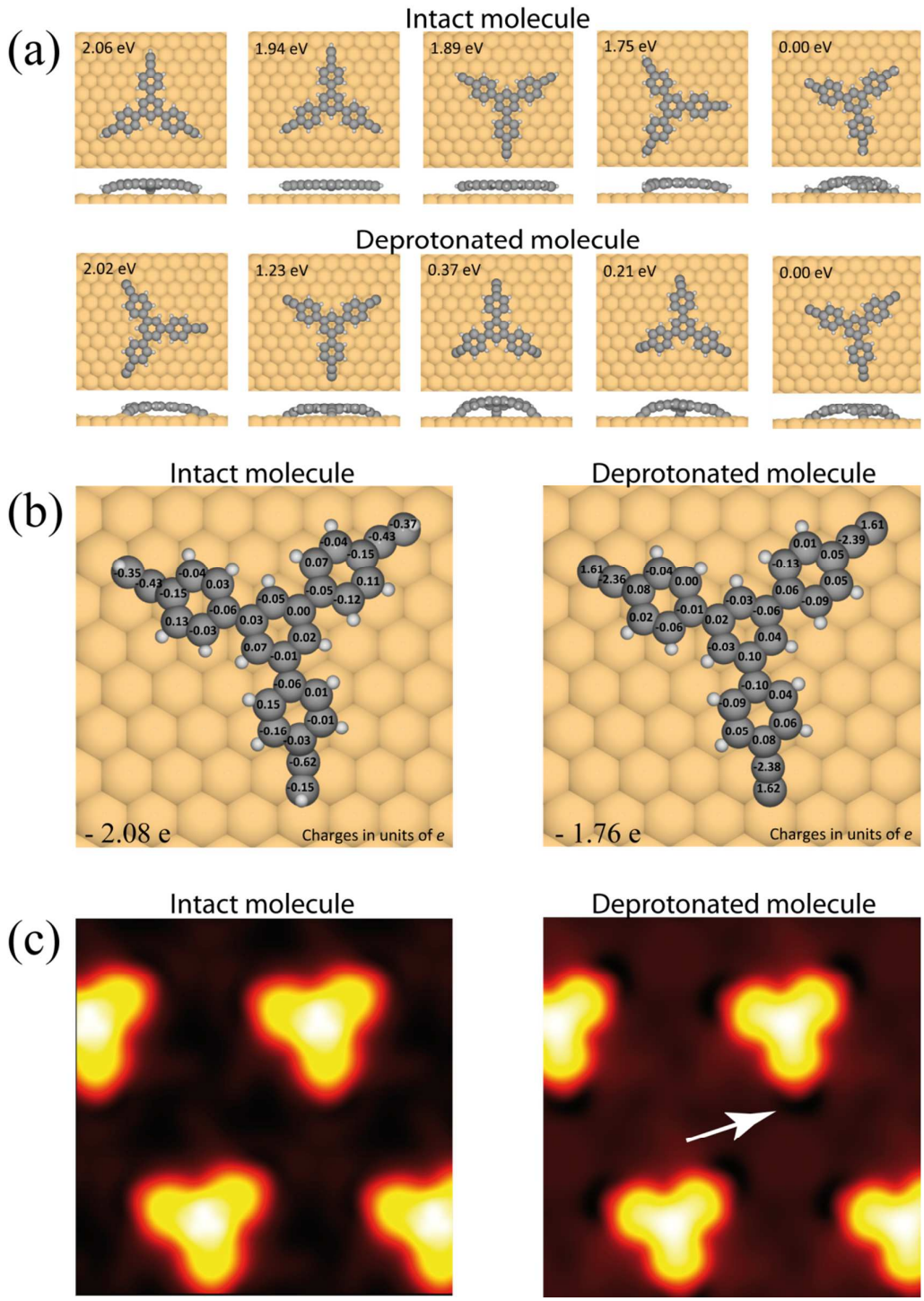

Figure S5. (a) DFT calculated geometries for intact Ext-TEB (upper panel) and triply deprotonated (lower panel) molecules on Cu(111), with energies indicated with respect to the most stable adsorption geometry for each species. Note that for the calculations of the relative energies the 1st Brillouin zone was sampled by the Gamma-point only. However, relative energies converge significantly faster than the adsorption energy, and by doing all calculations also for a 2×2 k-point sampling we could confirm that the relative energies reported here are converged well below 0.2 eV. Most importantly, the relative energies are

enough converged to conclude about the most stable adsorption site for the respective molecule. (b) Carbon-atom-wise Bader charge analysis of intact and deprotonated molecules on Cu(111). The total (including H atoms) Bader charges of intact and deprotonated Ext-TEB/Cu(111) are -2.08 e and -1.76 e, respectively. (c) DFT simulated STM images at bias U = -1.2 V for intact and deprotonated Ext-TEB molecules on Cu(111). The white arrow indicates the depression.

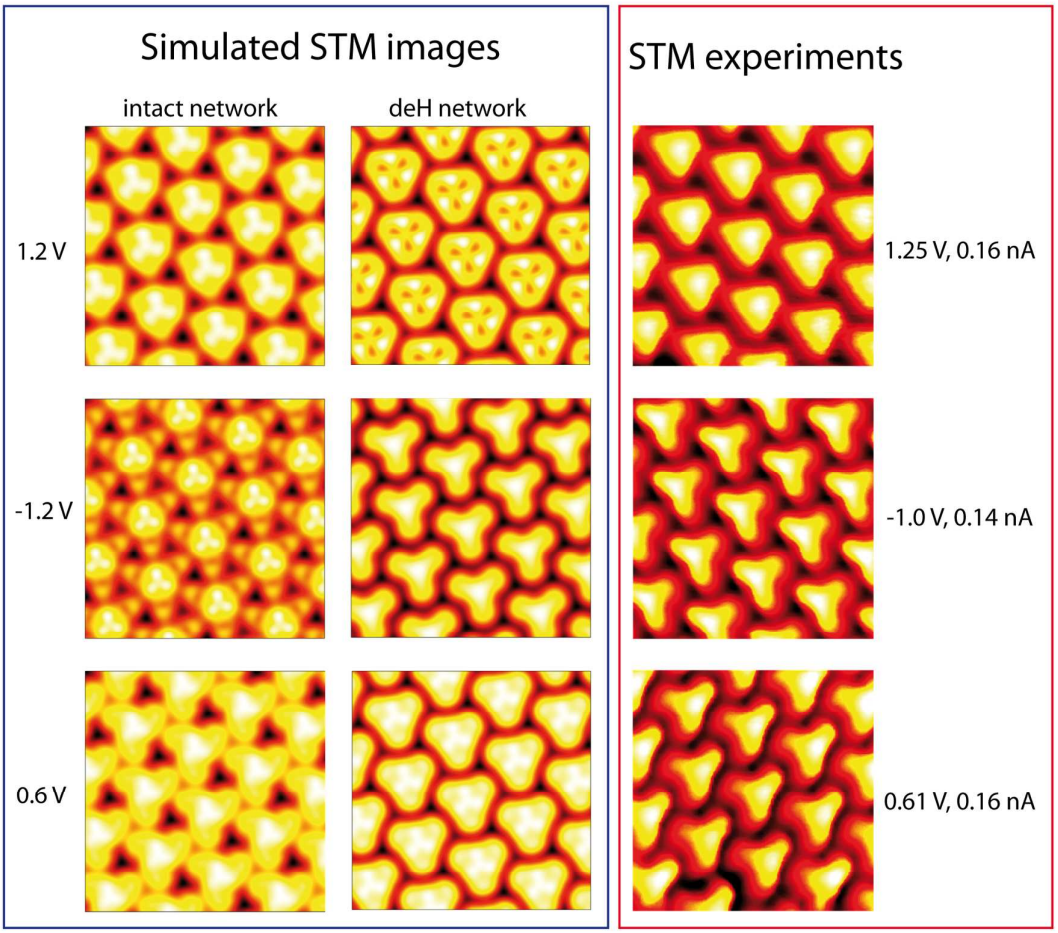

Figure S6. Simulated STM images for the intact and deprotonated molecular network at different biases (left), compared to the experimentally acquired images at similar biases (right). The theoretical images were obtained by integrating the local density of states from the Fermi level to different energies, as indicated. The size of the images is 5 × 5 nm^2.

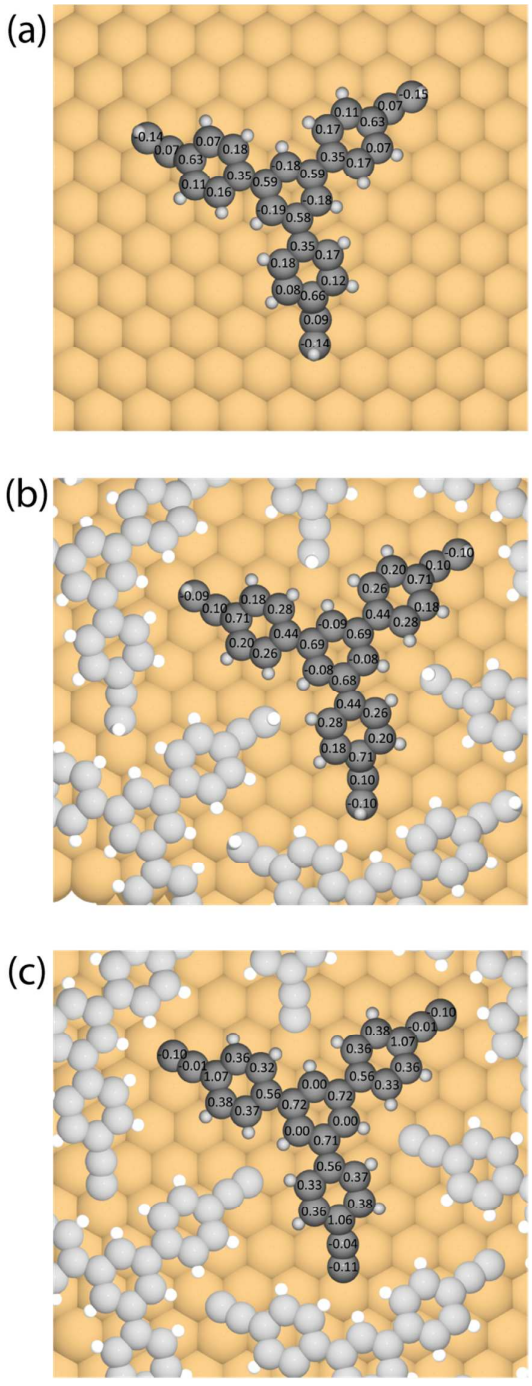

Figure S7. DFT calculated C 1s core-level shifts of isolated intact (a), intact network (b), and deprotonated network (c) of Ext-TEB molecules on Cu(111). Please note the distinction from the Bader charges depicted in Figure S5.

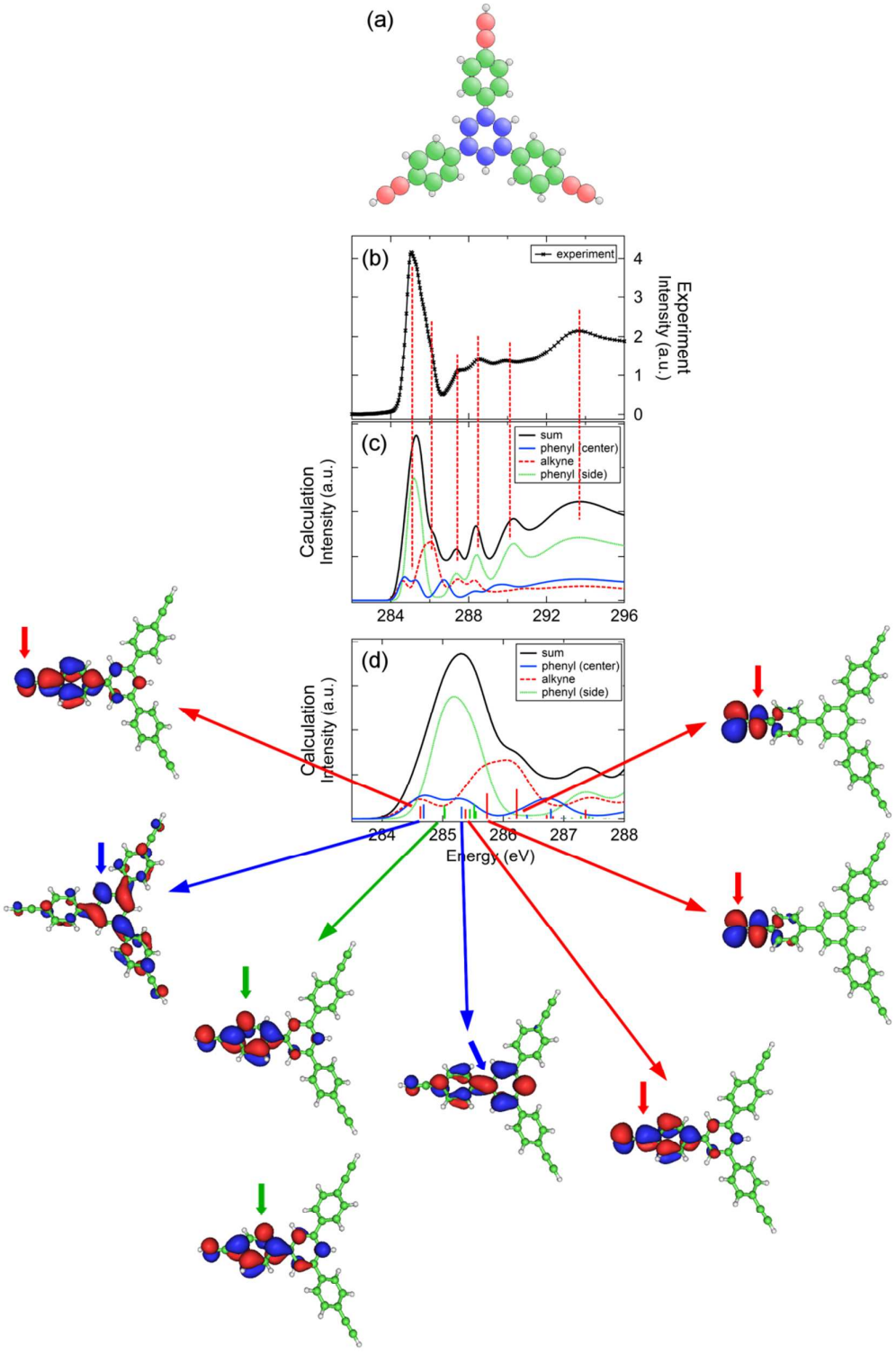

Figure S8. Comparison of (b) experimental and (c-d) simulated NEXAFS C K-edge spectra of (a) intact Ext-TEB. The experimental curve was recorded using an Ext-TEB multilayer sample grown on the Ag(111) surface where molecule-substrate interactions can be neglected. All experimental features are reproduced by the calculation (indicated by red dotted lines). (d) shows how the different parts of the molecules contribute to the main feature. The

corresponding transition potential final orbitals are displayed below. The arrows mark the respective excitation centers.

Computational details for Figure S8:

The calculations were performed using the DFT cluster code StoBe[1] and a revised PBE(RPBE) functional.[2,3] Only one isolated Ext-TEB molecule was taken into account for the calculation. The geometry optimization (using O-CARBON (7111/411/1) and O-HYDROGEN (3111/111) basis sets) resulted in a molecule with a flat central phenyl ring (blue in Fig. S8a) and rotated phenyl acetylene groups, as would be expected from steric considerations. For the simulation of the NEXAFS spectra within the transition potential (TP) approach[4] the excitation center was described with an IGLO-III basis set[5] and the other carbon atoms with effective core potentials. Additionally, a diffuse basis set was used to improve the description of the virtual orbitals. Further information on the general method can be found in Refs. 4 and 6. To facilitate the comparison with the experiment, the obtained discrete transition energies and intensities were broadened with Gaussian functions, using a FWHM of 0.6 eV up to the ionization energy E_{ion}, a linear increase from 0.6 to 6.5 eV in the region [E_{ion}, E_{ion}+10 eV] and 6.5 eV above (E_{ion} + 10 eV). To account for the missing core hole relaxation within the TP approach, a shift of -1.4 eV was applied to the simulated spectra which corresponds to the difference between the ionization energy obtained in the TP calculation and that determined by a ΔSCF calculation.

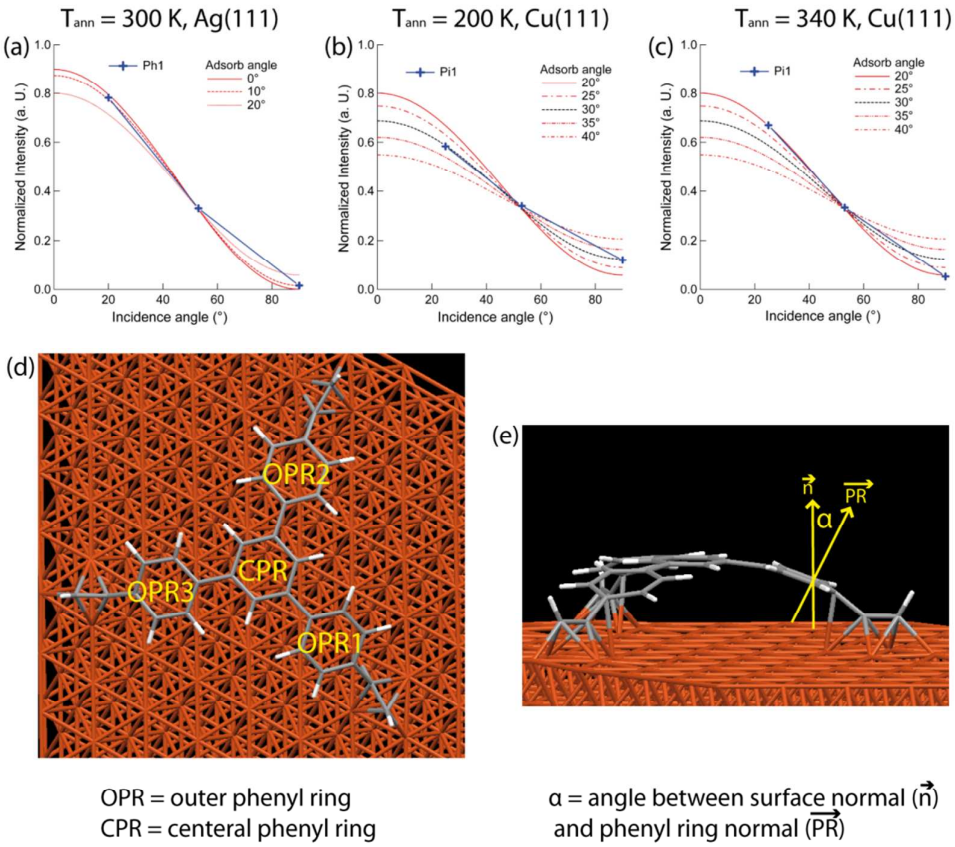

Figure S9: Angle dependence analysis of Ext-TEB (a) on Ag(111), monolayer sample prepared by annealing at 300 K, (b) on Cu(111) prepared at $T_{substrate}$ = 200 K, and (c) on Cu(111) after annealing at 340 K. (Measurement temperatures are mentioned in the experimental section.) (d) and (e) show that the phenyl ring tilt angle α is defined as the angle between the phenyl ring normal and the surface normal from DFT optimized models.

	OPR1(°)	OPR2(°)	OPR3(°)	CPR(°)	Average OPRs(°)	Average PR(°)
1. Isolated intact Cu(111)	18.78	17.84	18.01	1.26	18.21	13.97
2. Isolated de-H Cu(111)	11.91	12.14	12.12	0.15	12.06	9.08
3. Network intact Cu(111)	19.62	19.24	19.31	0.74	19.39	14.73
4. Network de-H Cu(111)	11.99	11.98	11.93	0.18	11.97	9.02
5. Isolated intact Ag(111)	1.00	0.80	0.08	0.15	0.63	0.51

Table S1. Phenyl ring tilt angles for four different DFT calculated geometries of Ext-TEB on Cu(111): (1) Isolated intact, (2) isolated deprotonated, (3) network intact, (4) network deprotonated; and one case on Ag(111): (5) isolated intact Ext-TEB on Ag(111). The tilting angle α of the phenyl ring is defined as the angle between the surface normal $\vec{n}$ and the phenyl ring normal $\overrightarrow{PR}$, shown in Figure S9(d-e).

Convergence with respect to k-point sampling

To justify the numerical accuracy of our reported energies we performed a careful control of the convergence with respect to the *k*-point sampling, both for isolated molecules and the intact molecular network. Fig. S10a shows the adsorption energy of an isolated intact Ext-TEB molecule as a function of *k*-point sampling. For a *k*-point sampling of 6×6 a convergence below 50 meV is obtained. Analogously, the formation energy of the intact Ext-TEB network is shown in Fig. S10b, for which a *k*-point sampling of 9×9 provides reaction energies converged below 10 meV.

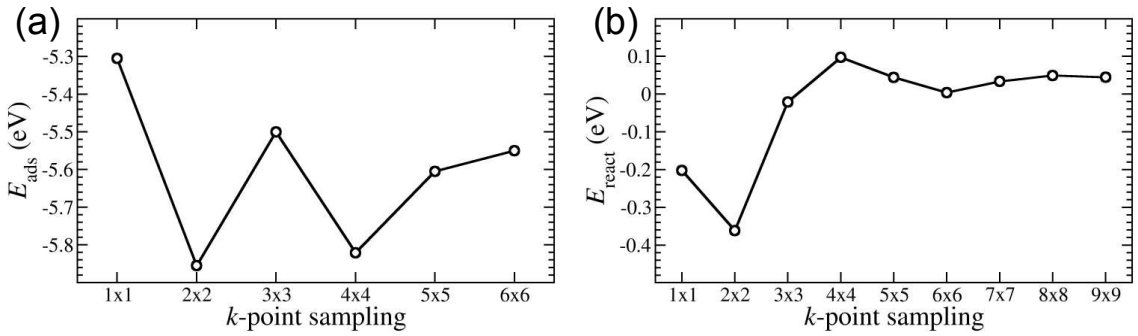

Figure S10. Convergence tests with respect to the *k*-point sampling: (a) The adsorption energy for an isolated intact Ext-TEB molecule adsorbed in its most favorable adsorption site. (b) The reaction energy for the formation of the network of the intact Ext-TEB network.

Analysis of surface corrugation

The calculated surface corrugation of 0.22 Å (see below) induced by alkynyl-surface interaction is only half the value typical for systems in which such surface-directed interactions play a relevant role for the assembly behavior see, e.g., tetracyano-*p*-quinodimethane on Cu(100)[7], accordingly we conclude that it contributes only little to the network stabilization.

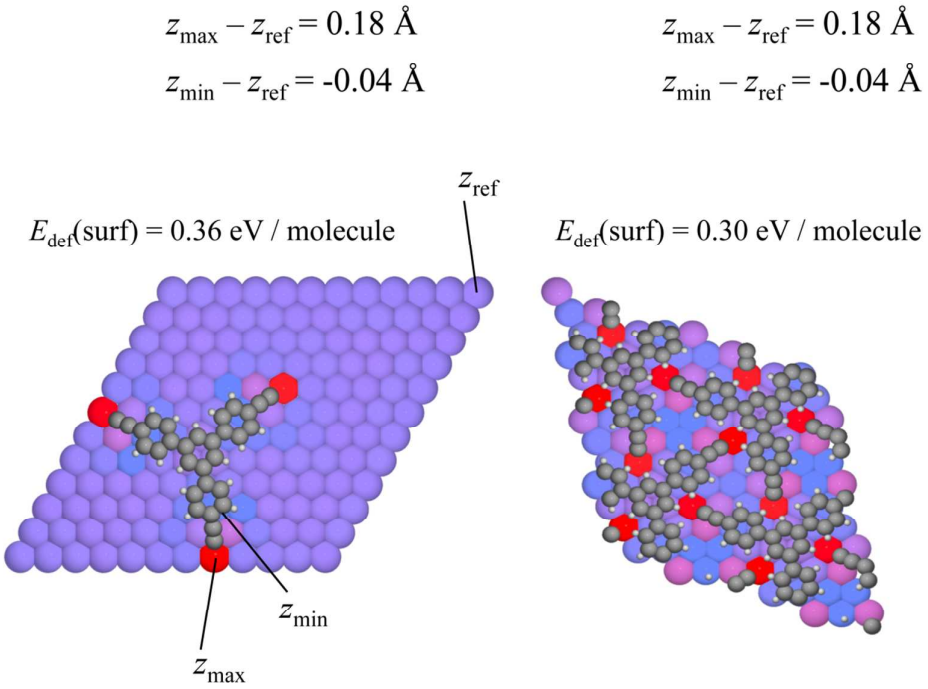

Figure S11. DFT calculated molecular adsorption induced surface corrugation as well as surface deformation energies for isolated deprotonated Ext-TEB on Cu(111) (left panel), and for deprotonated Ext-TEB network on Cu(111) (right panel). The red atoms have the largest z-components (furthest away from the underlying copper layers), while the bluish have the smallest z-component (closest to the underlying copper layers). z_{ref} is the reference atom for both system, which has the same z-components as the clean surface (within 0.01 Å).

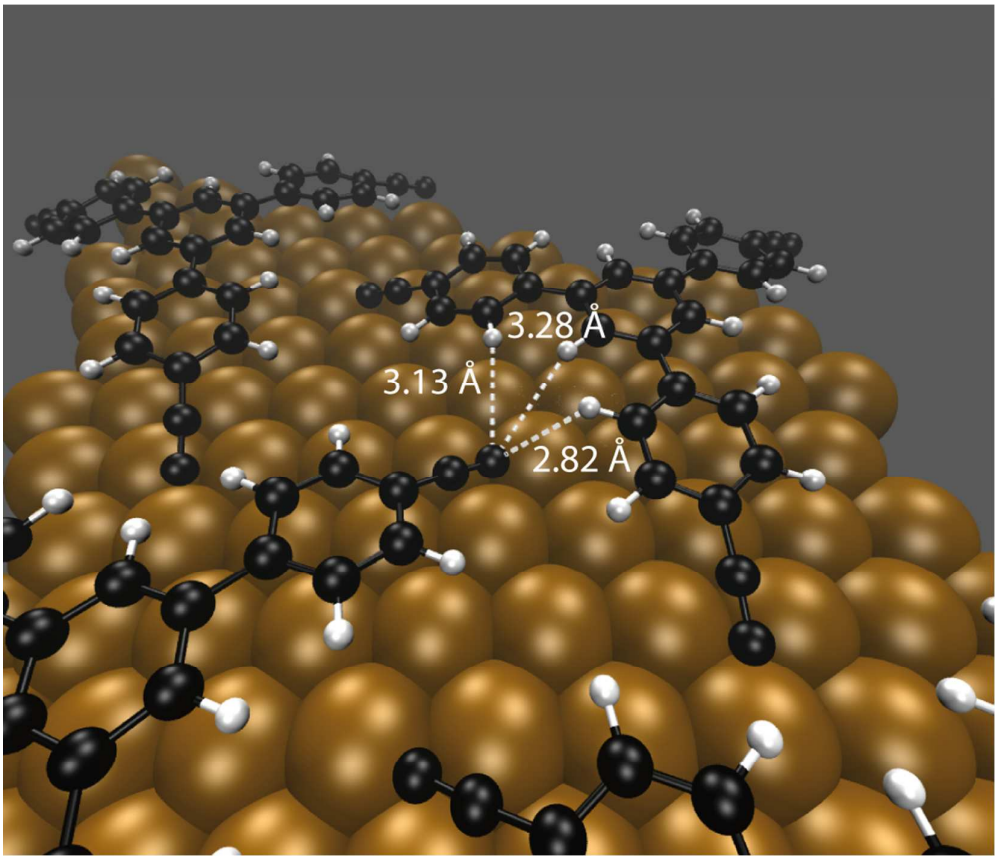

Figure S12. DFT optimized adsorption geometry of deprotonated Ext-TEB network on Cu(111). The distances of the terminal C atom at the alkynyl to three nearest H atoms are reported.

Analysis of van der Waals contribution

For the intact network, E_{tot} follows the E_{vdW} quite closely before the repulsive interactions set in. Therefore, the vdW interaction is the dominant attractive force for the intact molecules. For the dehydrogenated molecule, E_{vdW} is very similar to that of the intact network. However, the E_{tot} differs significantly from the E_{vdW} even at large distances, and there is an additional attractive component, which can be attributed to the electrostatic interaction between the π system of the radical alkynyl (·C≡C−R) and three neighboring hydrogens (C−H). For a negatively charged alkynyl group ($^{\delta-}$C≡C-R) on Cu(111) (cf. answer to question **3**), the electrostatic interaction must be strengthened.

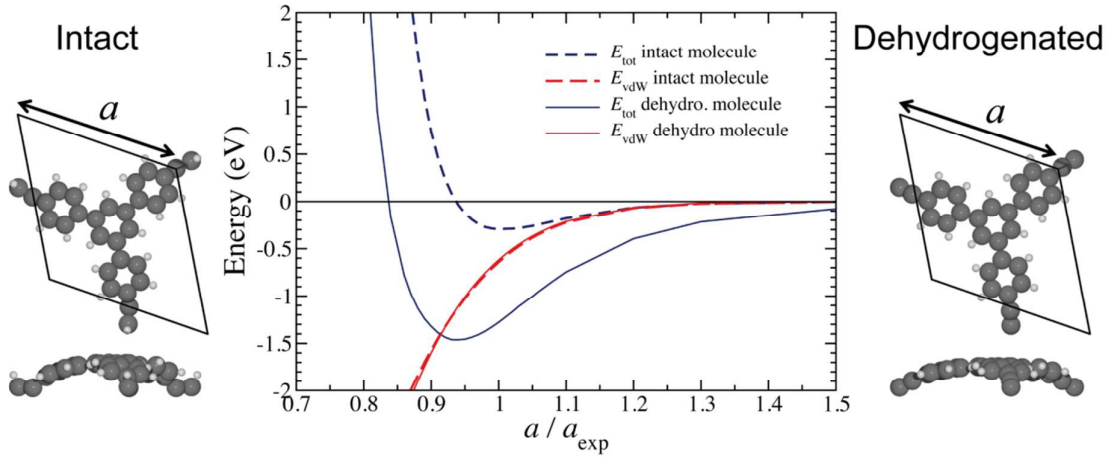

Figure S13. Calculations of freestanding ext-TEB molecules, with the molecular geometry frozen in that of the network on Cu(111), for intact and dehydrogenated molecules, respectively. Both networks are electrically neutral. The calculations were done for different lattice parameters *a* and the results are given with respect to the experimental lattice constant of the network on Cu(111). The total energy E_{tot} and the vdW contribution E_{vdW} to this energy are plotted.

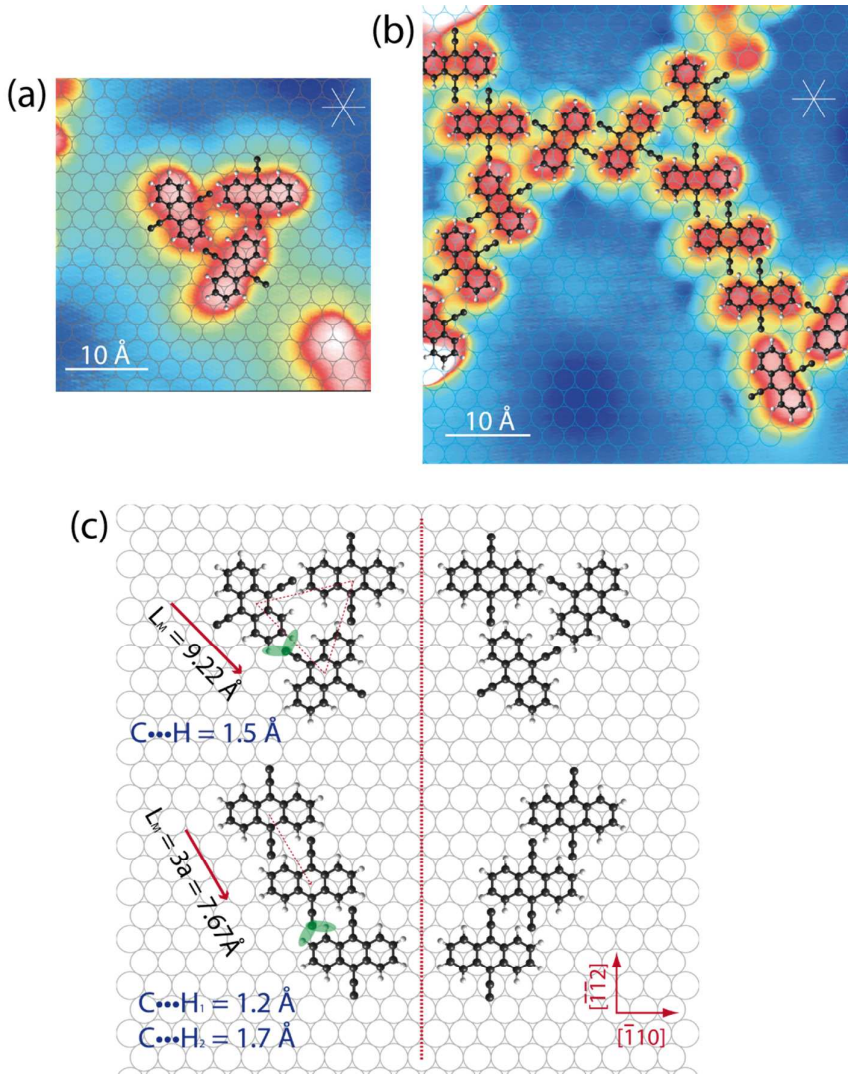

Figure S14. High-resolution STM image of DEAN on Cu(111) superimposed with planar DEAN gas phase model calculated by HYPERCHEM and the underlying Cu(111) lattice. (a) DEAN cluster, U_b = -0.25 V, I_t = 0.1 nA. (b) DEAN chains, U_b = -1.0 V, I_t = 0.08 nA. (c) Models including the mirror-symmetric enantiomorphs and C···H distances assuming a planar conformation for DEAN. The molecular adsorption sites are proposed.

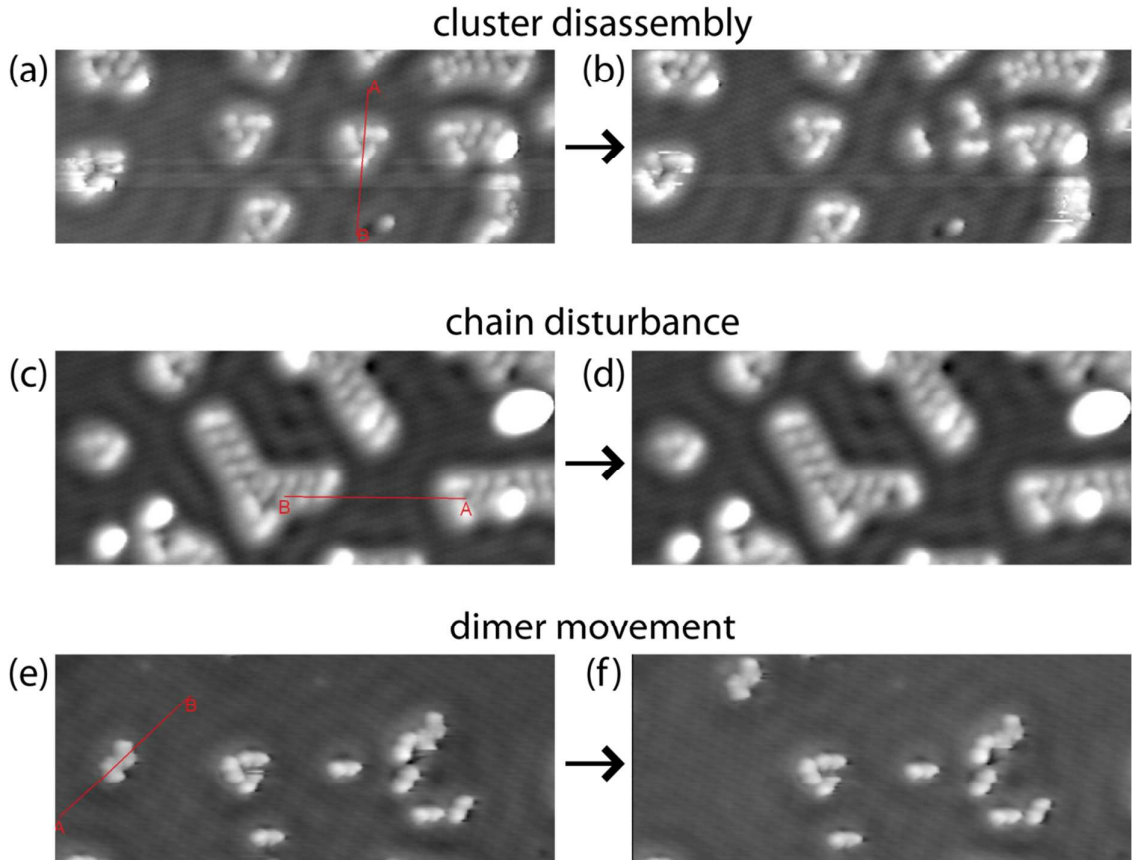

Figure S15. STM images before (left) and after (right) lateral molecular manipulation of DEAN on Cu(111), showing non-covalent character of the self-assembled cluster and chain. (a) and (b) display triangular cluster disassembly. (c) and (d) show that one end of the molecular chain is disturbed. (e) and (f) demonstrate the DEAN dimer moves as a unit.

References

(1) Hermann, K.; Pettersson, L. G. M.; deMon developers group *StoBe software V. 3.0, 2007; see http://www.fhi-berlin.mpg.de/KHsoftware/StoBe.*

(2) Perdew, J. P.; Burke, K.; Ernzerhof, M. Generalized gradient approximation made simple. *Phys. Rev. Lett.* **1996**, *77*, 3865-3868.

(3) Hammer, B.; Hansen, L. B.; Nørskov, J. K. Improved adsorption energetics within density-functional theory using revised Perdew-Burke-Ernzerhof functionals. *Physical Review B* **1999**, *59*, 7413-7421.

(4) Triguero, L.; Pettersson, L. G. M.; Ågren, H. Calculations of near-edge x-ray-absorption spectra of gas-phase and chemisorbed molecules by means of density-functional and transition-potential theory. *Physical review B* **1998**, *58*, 8097-8110.

(5) Kutzelnigg, W.; Fleischer, U.; Schindler, M. *The IGLO-Method: Ab-initio Calculation and Interpretation of NMR Chemical Shifts and Magnetic Susceptibilities.* In NMR Basic Principles and Progress; Springer Verlag, Berlin/Heidelberg, 1991; Vol. 23, p 165-262.

(6) Kolczewski, C.; Hermann, K. Ab initio DFT cluster studies of angle-resolved NEXAFS spectra for differently coordinated oxygen at theV(2)O(5)(010) surface. *Surf. Sci.* **2004**, *552*, 98-110.

(7) Tseng, T. -C.; *et al*, *Nat. Chem*. **2010**, 2, 374-379.